

DOI: 10.1002/((please add manuscript number))

**Article type: Full Paper**

**Engineering multicomponent hydrogel constructs for creating 3D vascularized bone**

*Mehdi Kazemzadeh-Narbat, Jeroen Rouwkema, Nasim Annabi, Hao Cheng, Masoumeh Ghaderi, Byung-Hyun Cha, Mansi Aparnathi, Akbar Khalilpour, Batzaya Byambaa, Esmail Jabbari, Ali Tamayol\*, Ali Khademhosseini\**

[\*] Corresponding authors: A. Tamayol, A. Khademhosseini

Dr. M. Kazemzadeh-Narbat, Dr. J. Rouwkema, Dr. N. Annabi, Dr. H. Cheng, Dr. M. Ghaderi, Dr. B. H. Cha, Dr. M. Aparnathi, Dr. A. Khalilpour, Dr. B. Batzaya, Dr. A. Tamayol, and Prof. A. Khademhosseini

Biomaterials Innovation Research Center

Department of Medicine

Brigham and Women's Hospital

Harvard Medical School, Boston, MA 02139, USA.

E-mail: [alik@bwh.harvard.edu](mailto:alik@bwh.harvard.edu) (A. Khademhosseini); [atamayol@partners.org](mailto:atamayol@partners.org) (A. Tamayol)

Dr. M. Kazemzadeh-Narbat, Dr. J. Rouwkema, Dr. N. Annabi, Dr. H. Cheng, Dr. M. Ghaderi, Dr. B. H. Cha, Dr. M. Aparnathi, Dr. A. Khalilpour, Dr. B. Batzaya, Dr. A. Tamayol, and Prof. A. Khademhosseini

Harvard-MIT Division of Health Sciences and Technology

Massachusetts Institute of Technology

Cambridge, MA 02139, USA.

Dr. A. Tamayol, Dr. N. Annabi, and, Prof. A. Khademhosseini.

Wyss Institute for Biologically Inspired Engineering

Harvard University, Boston, MA 02115, USA.

Prof. J. Rouwkema

Department of Biomechanical Engineering

MIRA Institute for Biomedical Technology and Technical Medicine

University of Twente

Enschede, The Netherlands

Prof. N. Annabi

Department of Chemical Engineering

Northeastern University

Boston, MA, 02115-5000, USA.

Prof. Esmail Jabbari  
Biomimetic Materials and Tissue Engineering Laboratories  
Department of Chemical Engineering  
University of South Carolina  
Columbia, South Carolina, 29208, USA

Prof. A. Khademhosseini  
Department of Physics  
King Abdulaziz University  
Jeddah 21569, Saudi Arabia

Prof. A. Khademhosseini  
Department of Bioindustrial Technologies  
College of Animal Bioscience and Technology  
Konkuk University  
Seoul, Republic of Korea

## **Abstract**

Engineering bone tissue requires the generation of a highly organized vasculature. Directing spatial cellular behavior and differentiation for creating mineralized regions surrounded by vasculature can be achieved by controlling the pattern of osteogenic and angiogenic niches. We engineered vascularized bone tissues by incorporating osteogenic and angiogenic cell-laden niches in a photocrosslinkable hydrogel construct. Two-step photolithography process was used to control the stiffness and distribution of cells in the patterned hydrogel and osteoinductive nanoparticles were utilized to induce osteogenesis. The size of microfabricated constructs had a pronounced effect on cellular organization and function. We showed the simultaneous presence of both osteogenic and angiogenic niches in one construct resulted in formation of mineralized regions surrounded by organized vasculature. In addition, the presence of neovasculature improved bone formation. The approach can be used for engineered constructs that can be used for treatment of bone defects.

**Keywords:** Bone tissue engineering; Micropatterning; Hydrogels; Vascularization.

## 1. Introduction

Even though bone tissue has a remarkable regenerative capacity, large bone defects are often unable to fully heal on their own because of the destruction of the local vascular network. <sup>[1, 2]</sup> Traditional approaches for management of large bone defects include autologous bone transplantation and cancellous bone allografts. <sup>[3]</sup> Autologous bone grafts, particularly vascularized grafts of the fibula and iliac crest, are effective in the treatment of large bone defects since they provide both an osteogenic environment and a vascular network. <sup>[4]</sup> However, their shortcomings remain an obstacle. Moreover, harvesting autografts is time consuming, expensive and associated with infection, pain, and hematoma and major microsurgical operative procedures are required for transplantation of vascular autografts. <sup>[3, 5]</sup> In addition, allografts carry the risk of immune rejection. <sup>[6-9]</sup> Thus, a new paradigm is required for treatment of large bone defects.

Tissue engineering promises an alternative solution for the treatment of large bone defects. According to preclinical reports, cell-based tissue-engineered constructs are capable of inducing more bone formation compared to acellular constructs. <sup>[10]</sup> By combining patient-derived cells with biomaterial scaffolds and/or extracellular matrix (ECM) analogues, large volumes of tissue analogues can be prepared. <sup>[11, 12]</sup> However, these strategies have not been successful in accommodating proper vasculature to compensate slow invasion/perfusion of the host vasculature into the scaffold. <sup>[1, 8, 11, 13]</sup> This results in ischemia and subsequently poor cell survival and function within days of implantation. <sup>[14, 15]</sup> Thus, engineering strategies to enhance vascularization has been the focus of several studies. <sup>[15, 16, 17]</sup> The strategies followed in these studies can be broadly divided into two groups: 1) to engineer prevascularized constructs so that they can develop angiogenic cues through their encapsulated cells and, 2) employing biological processes for self-formation of effective vasculature. <sup>[18, 19]</sup> However, there are limitations for

either of these approaches, such as poor resolution of fabricated vascular patterns and inability to direct the organization of the formed structures respectively. <sup>[1, 6]</sup> A promising approach to address these challenges is to engineer tissue constructs with predefined spatial distribution of angiogenic cues to direct the architecture of the formed vasculature. <sup>[18]</sup> Even though studies on pre-vascularized bone tissue engineering have been successful in showing the potential of this approach, parallel optimization of both osteogenesis and angiogenesis has proven difficult. <sup>[10, 20, 21]</sup> The two tissue structures require different microenvironments with regards to biomaterial chemistry, matrix mechanical properties, and the availability of morphogens and growth factors. <sup>[8, 22]</sup> This is unattainable using standard tissue engineering protocols, where all cells are mixed and therefore experience the same external cues. A methodology that is capable of patterning local environments within a single tissue construct would allow for the optimization of conditions for both tissues, while still benefiting from the interactions between the different cell types. Approaches where growth factors are patterned within hydrogels in order to achieve engineered bone tissue containing a microvascular network have for instance been investigated (PMID: 26693678 and PMID: 26721447) Coupling osteogenic and angiogenic cues in a scaffold can potentially form an early vascular network by encapsulated cells preventing an ischemic environment to sustain cellular viability in non-healing defects. An engineered biomaterial for this purpose should be able to mimic the natural bone ECM to promote bone healing as well as enhance 3D vascular network formation. <sup>[23]</sup>

Co-culture studies of osteogenic and endothelial cells have also shown that these systems result in an upregulation of both osteogenesis and angiogenesis, due to an intricate growth factor interaction between the two cell types. <sup>[10, 20, 21]</sup> These synergistic interactions between osteoblasts/osteogenic precursors and endothelial cells significantly improve the development of a vascular network that serves as a template for later ossification. <sup>[24]</sup> Apart from that, mesenchymal stem cells (MSCs), which are generally used as osteoprogenitor cells in these systems, can differentiate towards smooth muscle cells or pericytes, and

can stabilize the formed vascular structures when cultured in direct contact with endothelial cells in defined conditions. <sup>[18, 21, 25]</sup> Correia et al. showed that the vascular structures formed by Human umbilical vein endothelial cells (HUVECs) were only stable when they were co-cultured with human MSCs (hMSCs). <sup>[20]</sup> *In vivo* studies have shown that endothelial cells co-cultured with hMSCs generate more robust vascular networks that can anastomose to the host vasculature. <sup>[26]</sup> Our group previously demonstrated that the co-culture of endothelial cells with hMSCs in a hydrogel system significantly enhanced the formation of stable capillaries. <sup>[27, 28]</sup>

Due to recent advances in microfabrication approaches, it is possible to integrate microvasculature in engineered tissues with spatial and temporal control over micropatterns. <sup>[29]</sup> Photocrosslinkable hydrogels provide flexibility to enhance architecture of the micropatterns. <sup>[30, 31]</sup> Gelatin methacryloyl (GelMA) is a non-cytotoxic and biodegradable hydrogel modified with methacryloyl groups, which has attracted significant attention in tissue engineering due to its photocrosslinkable properties and tunable mechanical robustness while retaining cell-binding motifs. <sup>[27, 31, 32]</sup> Interestingly, GelMA can be polymerized *in vivo*, allowing for the creation of vascular networks *in situ* (PMID: 23773819). GelMA constructs have been photopatterned to generate highly organized 3D vasculature through HUVECs encapsulation in the hydrogel prepolymer. It was shown that varying the width and height of beams could significantly alter HUVEC alignment within the micropatterned. <sup>[33]</sup> Although, an organized vasculature was formed by using this method, the potential of integrating the engineered vascular network with another tissue construct (e.g. bone) to engineer a vascularized tissue was not explored.

The objective of this work was to engineer a 3D construct containing vasculogenic and osteogenic niches using photolithography and to study its potential for formation of vascularized bone tissue. The engineered construct has the potential to be used along with scaffolds for the treatment of large bone defects.

## 2. Results and Discussion

### 2.1. Fabrication of cell-laden micropatterned constructs

Native bone tissue receives nutrients and oxygen through an organized vasculature. Therefore, engineering a functional bone tissue requires the formation of a biomimetic and organized vasculature. [2, 15] We hypothesized that engineering a construct that permits simultaneous osteogenesis and angiogenesis in predefined patterns would address this challenge. [6, 17] In this study, GelMA, which is a photopolymerizable hydrogel comprised of modified natural ECM components, was used as a material for both osteogenic and angiogenic niches. GelMA can be micropatterned using photolithography into a variety of shapes and configurations, without reducing cellular viability and function. [31, 34, 35, 36]

A two-step photolithography process was used in this work to form spatially organized vascular networks inside an osteogenic niche (**Figure 1**). [37] Micropatterned vascular networks formed by endothelial and MSCs inside GelMA in a precise and concentric fashion, strengthened by a secondary crosslinking step forming the osteogenic niche containing bone forming cells encapsulated in GelMA (**Figure 1**). Although numerous approaches have been developed to create a vascularized bone constructs, [27, 38] relatively few studies have considered mimicking the 3D bone architecture by forming endothelial cord-like vasculature within the bone forming hydrogel microstructure.

Several studies have shown that vascular endothelial growth factor (VEGF) recognized as an angiogenic protein regulates endothelial cell (i.e. HUVECs) proliferation and promote osteogenesis by reciprocal regulation between osteoblasts and endothelial cells [7, 18, 39]. It has been reported that hMSCs exhibit an angiogenic potential and considerable synergism when co-cultured with endothelial cells. However specifically defined media are essential to encourage hMSCs to differentiate into mural cells and co-localize with capillary-like structures. In terms of media ingredients, some studies have disputed VEGF

as the most important growth factor regulating this differentiation <sup>[18, 40]</sup>. Therefore the applied growth media in this work was optimized based on the quantity of VEGF in Endothelial Cell Growth Medium (EGM<sup>TM</sup>-2 BulletKit<sup>TM</sup>, Lonza) in order to enhance vascularization while maintaining the growth of osteogenic cells. It has also been reported that co-delivering VEGF and osteogenic agents within separate niches enhances bone regeneration <sup>[41]</sup>. Therefore, the effect of loading both silicate nanoplatelets (Laponite) and tricalcium phosphate ( $\beta$ TCP) nanoparticles <sup>[42]</sup> into the osteogenic niche to induce osteogenesis was studied (**Figure 1**). We have previously reported that Laponite with large surface area ( $> 350 \text{ m}^2 \text{ g}^{-1}$ ) and approximately 25 nm diameter and 1 nm thickness, possessing a negative face charge and a weak positive rim charge, are able to induce osteogenic differentiation in the absence of any additional osteoinductive factor. <sup>[43]</sup>

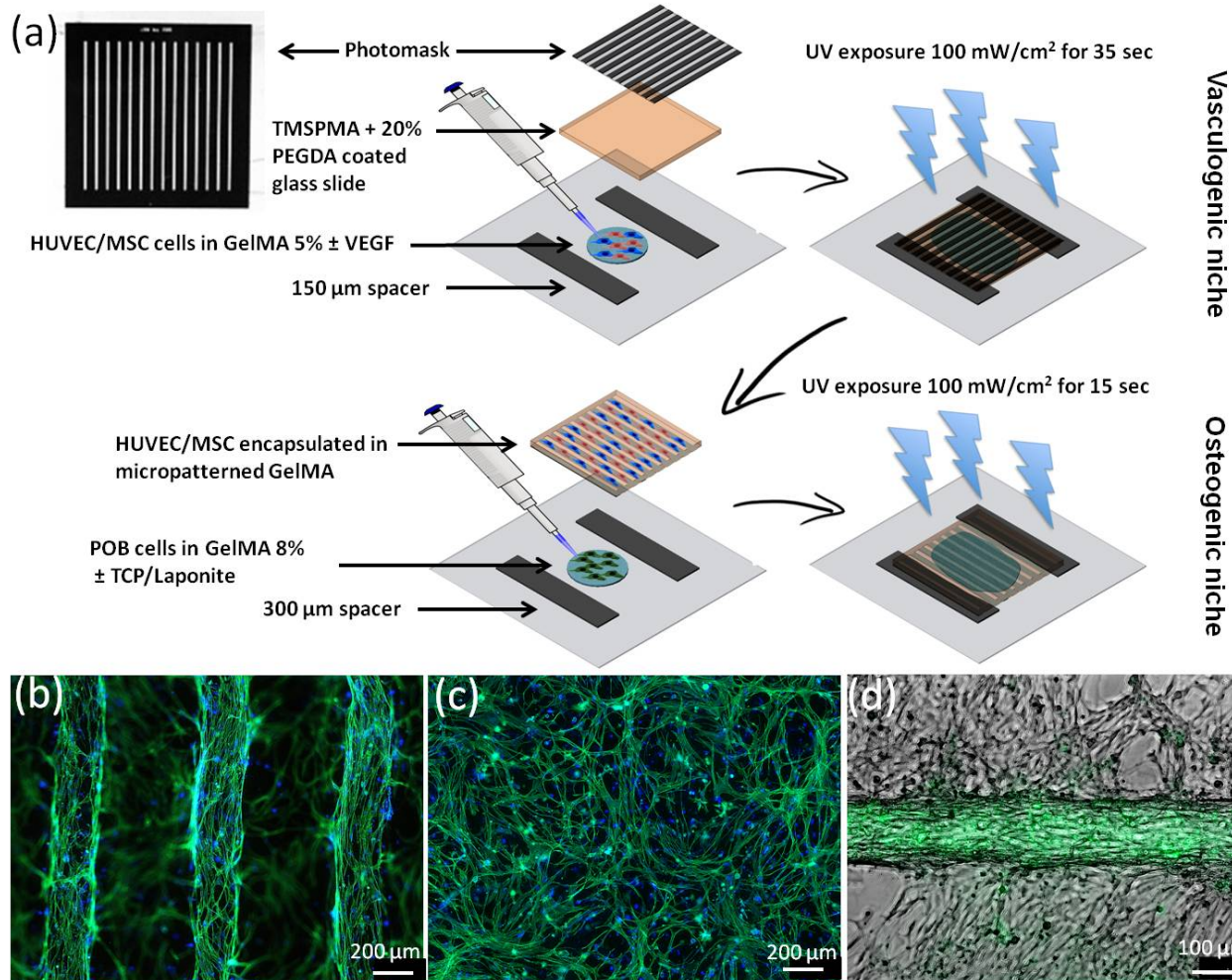


Fig 1. (a) Schematic representation of cell-laden micropatterned organized vascular networks and osteogenic niche fabricated using direct polymerization through photomasks, (b) actin filaments and DAPI stained HUVECs/hMSCs (1:1) encapsulated in unpatterned GelMA hydrogel, (c) micropatterned GelMA hydrogel containing HUVECs/hMSCs (1:1), (d) combined angiogenic niche containing HUVECs/hMSCs (1:1) co-culture in GelMA 5% and osteogenic niche containing preosteoblasts (POBs) in GelMA 8%.

## 2.2. Engineering the angiogenic niche

Encapsulated cells readily elongated, proliferated, and migrated when embedded in microfabricated GelMA hydrogels, indicating that the cells adhered to the hydrogel matrix. Cell alignment plays a critical role in many components of tissue microarchitecture. Several studies have reported the cell alignment through local tension lines and along free boundaries such as grooved surfaces, microfibers and micropatterns. [36, 40, 44, 45-47]. Here, we used a photomasking technique and micropatterned geometric



restriction to create an aligned 3D spatial organization of vascular microstructures without the application of any additional stimuli.

Fluorescence images of HUVECs and hMSCs exhibited a rounded morphology of cells on day 1 and elongated and spindle-like morphology aligned along the direction of the micropatterns on day 3. On day 5 interconnection of neighboring cells with the formation of cord-like structure was observed on the patterned gels (Figure 1b). As expected, randomly distributed cells were observed within the unpatterned regions of the 3D microenvironment of the GelMA construct (Figure 1c).

To investigate the effect of micropattern size on cellular alignment, HUVEC/hMSC-laden micropatterned hydrogels with varying beam widths (50, 150, and 300  $\mu\text{m}$ ) were prepared using photolithography. Successful inclusion of homogeneously distributed cells within the micropatterns was confirmed by fluorescence microscopy. Within 5 days of culture, the microconstructs were filled with cells which aligned along the direction of the patterns with depended on the size of geometrical features, as shown by filamentous actin and nuclear staining (**Figure 2a**). It was observed that cellular alignment had an inverse relationship with dimension of the patterns. High degrees of cell alignment was observed for 50  $\mu\text{m}$  (up to  $80 \pm 7.6\%$  for  $<10^\circ$ ), and 150  $\mu\text{m}$  (up to  $63 \pm 2\%$  for  $<10^\circ$ ), while the 300  $\mu\text{m}$  beam size exhibited almost random orientation of cells and only those in close proximity to the perimeter tended to align along the long-axis of the micropatterns (**Figure 2b**).

Confocal microscopy was used to assess 3D actin cytoskeleton organization and demonstrated that cells reorganized toward the periphery of the hydrogel constructs and self-assembled to form cord-like structures after 5 days of culture (**Figure 2c**). It should be noted that the structures as seen in figure 2c are filled with hydrogel and are therefore not perfusable as is. However, upon degradation of the hydrogel, open channels surrounded by endothelial cells will be attained. Optimal 3D cord and tubular structures with more circular cross-section profiles were observed for 150  $\mu\text{m}$  beam size (**Video S1**,

**Supporting Information**). Therefore, the microconstruct with 150  $\mu\text{m}$  geometrical feature was chosen for the rest of studies. Studies have shown that when endothelial cells are patterned, mechanical stresses generated by traction forces will cause a higher stress concentrated on the periphery of the features. This in turn initiates patterned proliferation, which triggers tube morphogenesis during angiogenesis. This effect is critical after implantation as the luminal structure can connect to vasculature of the patient and contribute in nutrient transport and survival of the cells. [50]

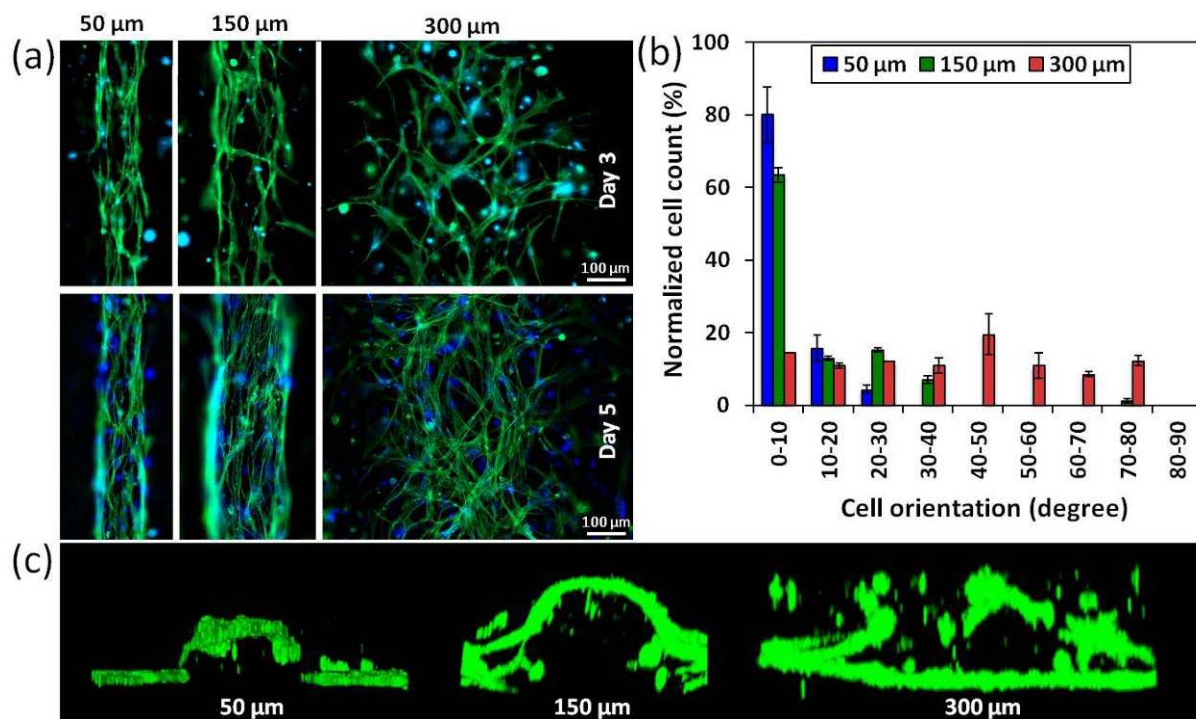


Fig 2. 3D cord formation and alignment of actin filaments (green) and DAPI (blue) stained HUVEC/hMSC in the micropatterned GelMA hydrogel. (a) Effect of pattern size on cell alignment using HUVEC/hMSC-laden GelMA gel with 50 and 150  $\mu\text{m}$  micropatterned beams. (b) Quantification of cell alignment at day 3 based on beam sizes. Error bars show the standard deviations between different trials. (c) Representative confocal images (video can be viewed in Supporting Information) from the cross-section of actin filaments stained HUVECs/hMSCs-laden micropatterned GelMA constructs, showing more stable 3D cord-like structure was created at 150  $\mu\text{m}$  (scale bars: 100  $\mu\text{m}$ ).

To further assess the behavior of HUVECs and hMSCs when encapsulated individually or in co-culture in 150  $\mu\text{m}$  micropatterns, the cell filamentous actin and nuclei were stained after 1, 3 and 5 days of culture

(Figure 3a). As shown in Figure 3b,c, both mono- and co-culture cells were highly aligned and elongated in patterned GelMA hydrogel and no significant difference was observed between mono- and co-cultures. In patterned constructs on day 5, more than 85% and 95% of co-culture cells aligned at  $<10^\circ$  and  $<20^\circ$  deviation from the direction of the micropatterns axis, respectively. This result indicated that micropatterning can significantly enhance the cell alignment and elongation on both mono and co-cultures within the hydrogel and form highly organized vascularized network. This is consistent with other *in vitro* and *in vivo* studies indicating the ability of MSCs to assist HUVECs in forming and maintaining a network when co-cultured with hMSCs in a hydrogel. In a similar study by Tsigkou *et al.* much shorter and wider multicellular cords were reported in mono-cultures of HUVECs than those formed by hMSC-containing cultures. [7]

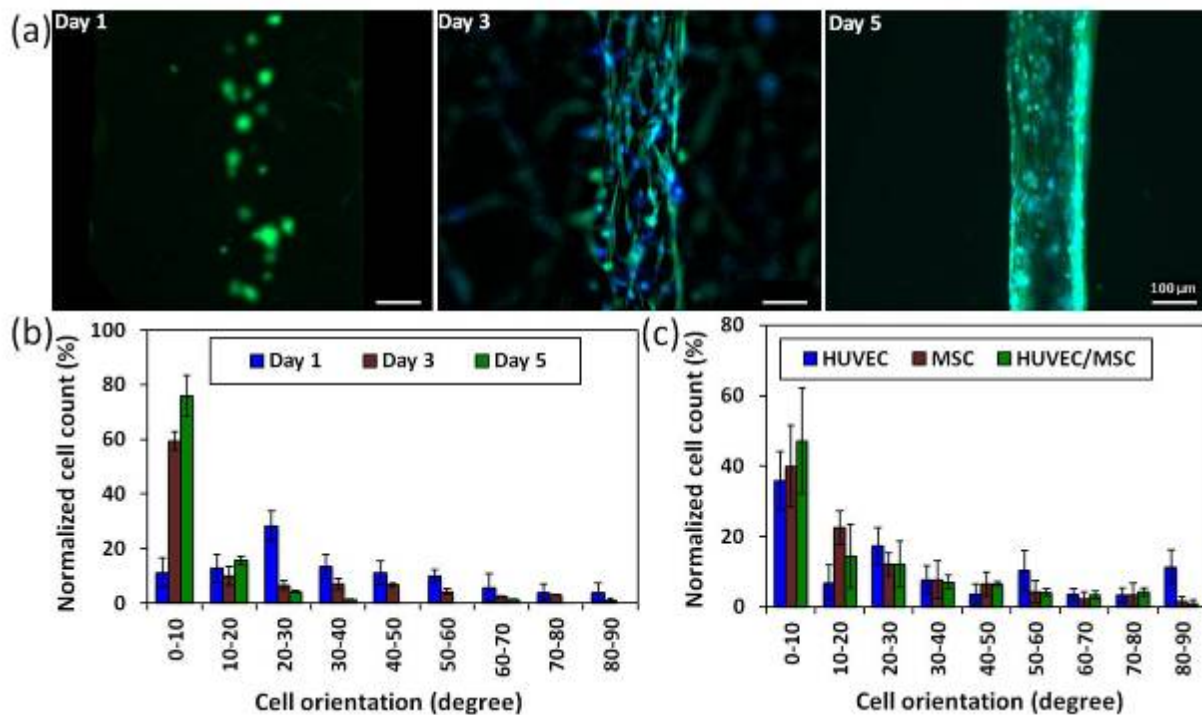


Fig 3. Cells cytoskeletal actin filaments alignment in 150  $\mu\text{m}$  micropatterned GelMA construct. Alignment analysis of cell within (a) micropatterned regions of 5% (w/v) GelMA hydrogel after 1, 3 and 5 days of co-culture as obtained by photomasking technique. Representative fluorescence images demonstrate DAPI-stained cell nuclei with cytoskeletal actin filaments orientation within patterned regions of the hydrogel. (b) Micropatterning significantly enhanced cell alignment in co-culture, more than 85% and 95% of co-culture cells aligned at  $<10^\circ$  and  $<20^\circ$  angles deviation from the direction of the

micropatterns on Day 5, respectively. (c) Both mono- and co-culture cells were aligned and elongated in patterned GelMA (scale bars: 100  $\mu\text{m}$ ).

To investigate pattern fidelity, defined as the number of cells migrating from micropatterns, three groups of cell-laden samples were studied including mono-culture of GFP-HUVECs, hMSCs labeled with DiD (Vybrant, Thermo Fisher Scientific), and co-culture of GFP-HUVECs/hMSCs. Consequently the amount of migrated cells from micropatterns was calculated relative to the total number of cells. It was observed that hMSCs and GFP-HUVECs had the highest (~55%) and lowest (~10%) tendency to migrate respectively, with an intermediate value for cell migration for co-culture of GFP-HUVECs/MSCs (~30%) (**Figure 4**). Overall, these data clearly indicate that the elongation, alignment and migration responses could be controlled and directed through optimization of the micropatterning conditions and encapsulated cells.

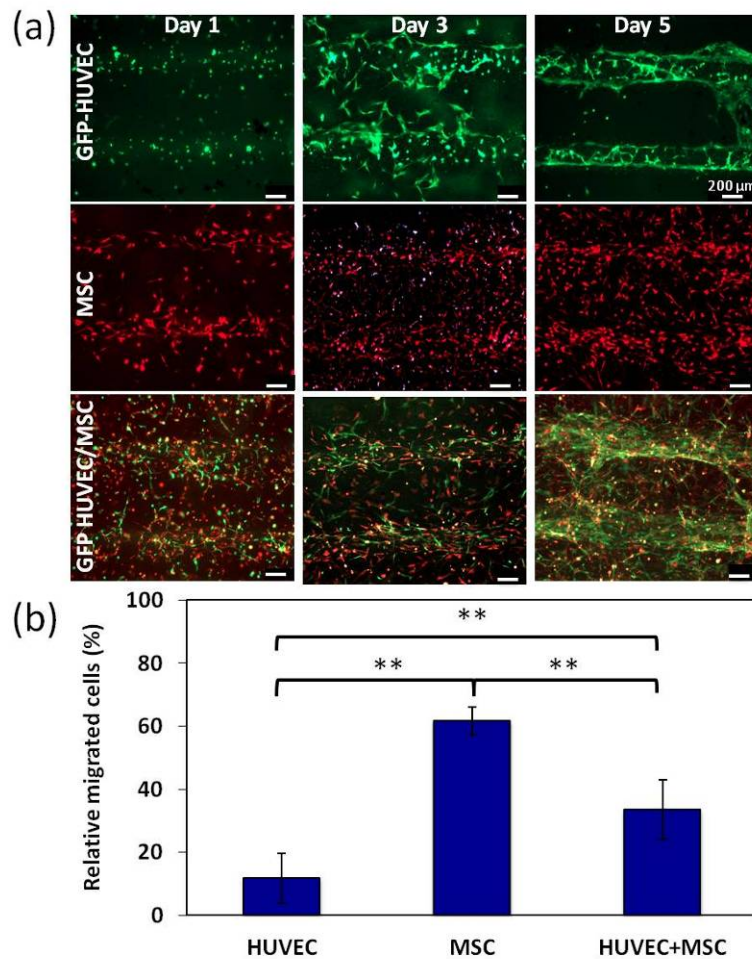


Fig 4. Cell migration from micropatterns. (a) Cell migration after 1, 3 and 5 day. (b) Quantification of relative migrated cells after 3 days. Relative migration indicates the relative number of migrated cells to the total number of cells. hMSCs and GFP-HUVECs showed the highest (~55%) and lowest (~10%) tendency to migrate and GFP-HUVECs/MSCs co-culture was somewhat in between (~30%). Columns indicate the values from six experiments; bars, SD. \*\* $P < 0.01$  as compared (Scale bars: 200  $\mu\text{m}$ ).

Maintaining normal cellular behavior in a 3D microenvironment is an important criterion for the fabrication of tissue constructs. [45, 51] The viability and proliferation of HUVECs and co-cultures of HUVECs/hMSCs with and without VEGF within micropatterns were assessed after 1, 3 and 5 days of culture. High viability of encapsulated cells was observed in patterned and unpatterned cell-laden GelMA and cells populated the constructs during the culture time. However, a significant increase in cellular metabolic activity and proliferation in co-cultures was observed compared to HUVECs mono-cultures

on day 5 as confirmed by a PrestoBlue<sup>®</sup> assay (**Figure 5b**). Over 90% cell viability was observed within the microconstructs by using a LIVE/DEAD assay as shown in **Figure 5a**, confirming the cytocompatibility of the fabrication process.

It is known that crosstalk between endothelial cells and hMSCs results in the differentiation of stem cells towards smooth muscle cells that later wrap endothelialized channels to form functional vessels. Thus, we performed immunostaining against an endothelial marker (CD31) and a smooth muscle marker ( $\alpha$ SMA). CD31, known as platelet endothelial cell adhesion molecule 1 (PECAM-1), is expressed on the surface of endothelial cell intercellular junctions and  $\alpha$ SMA is a marker for mural cells and is a major constituent of the contractile apparatus within these cells. Contractile cytoskeletal protein  $\alpha$ SMA, is the earliest marker of smooth muscle cell differentiation, which are present in both small and large blood vessels. The micropatterned constructs were CD31 and  $\alpha$ SMA positive at day 5 by immunostaining (**Figure 5d,e,f**). The expression of  $\alpha$ SMA confirmed that hMSCs differentiated to mural cells to stabilize the engineered vascular network. We have previously observed that co-cultures of hMSCs and HUVECs in hydrogel resulted in the formation of these stabilized vascular networks but the vasculature was randomly generated in bulk GelMA hydrogel [52]. To further assess the vascular stability, the expression of endothelial intercellular junctional protein VE-cadherin was examined after two weeks of culture (**Figure 6b**). Visualization of CD31 and VE-cadherin within the micropatterned hydrogel constructs confirmed that the HUVECs co-seeded with hMSCs formed vascular structures that exhibited mature intercellular junctions. Thus, micropatterning enabled us to engineer more organized vascular networks with the micropatterned HUVEC/hMSC-laden GelMA gel.

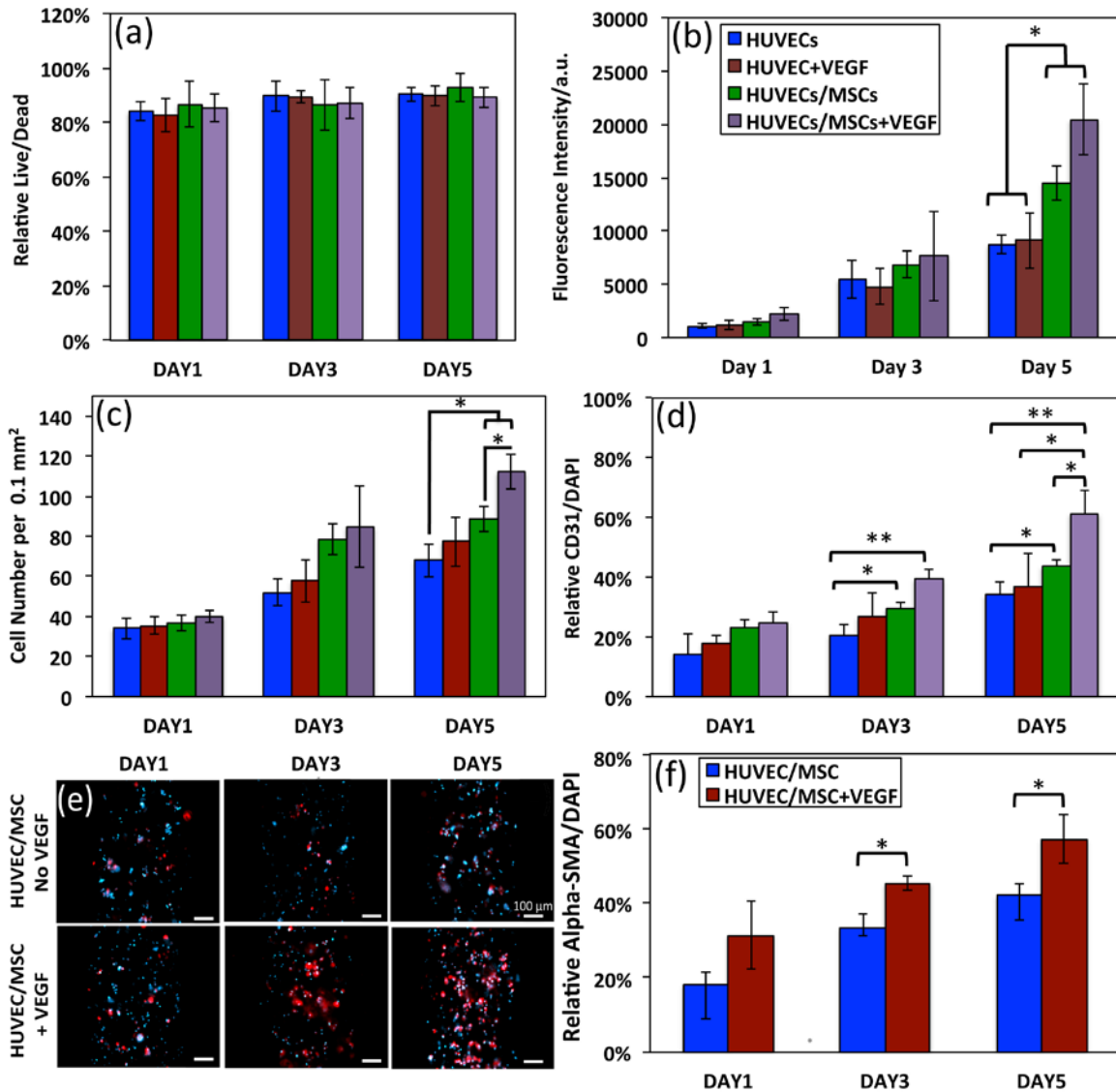


Fig 5. (a) Live/Dead cell viability assay shows >90% viability after 5 days. (b) PrestoBlue<sup>®</sup> metabolic assay indicates significant proliferation of co-culture. (c) Total cell quantification of DAPI-stained cells confirms the high proliferation. (d) Higher amount of CD31 expression was observed in the co-culture indicating higher endothelial activity. (e) Effect of VEGF on  $\alpha$ -SMA expression in HUVEC/hMSC co-culture. (f) Quantification of relative  $\alpha$ -SMA shows higher expression of  $\alpha$ -SMA, defined as the percentage of cell nuclei that co-localize with positive staining for  $\alpha$ -SMA. Columns indicate the values from six experiments; bars, SD. \*  $p < 0.05$  and \*\* $p < 0.01$  as compared.

### 3. Vascularized bone tissue constructs:

Higher concentration of GelMA (8 % (w/v)) was utilized to form osteogenic constructs including POB-laden hydrogel around micropatterned vascular network. This results in a higher stiffness for the



osteogenic environment, which has been shown to be beneficial for the osteogenic differentiation of hMSC.<sup>[53]</sup> The fabrication of combined angiogenic and osteogenic niches was successfully achieved with a two-step process, where HUVECs/hMSCs-laden micropatterned GelMA lines were covered with a layer of POB-encapsulated GelMA hydrogel (**Figure 6a**). The construct was then cultured in the optimized EGM2 media containing VEGF (**Figure S1, Supporting Information**) for 21 days.

The osteogenic differentiation in the POB-laden GelMA regions was confirmed by staining the calcified matrix with Alizarin Red (**Figure 6c,d**). This mineralization assay demonstrated high Alizarin Red absorbance from samples containing  $\beta$ TCP in comparison to Laponite and control. However this difference was expected due to the high concentration of calcium in  $\beta$ TCP as confirmed by a control with  $\beta$ TCP but without cells. Although mineralization was not significant in comparison to the control but stronger POB osteoinduction was observed from silicate nanoparticles (Laponite) in comparison to  $\beta$ TCP nanoparticles. Real-time polymerase chain reaction (qPCR) analysis indicated that osteogenic genes such as osteocalcin (OCN), RUNX2, osteopontin (OPN) and alkaline phosphatase (ALP) were upregulated in the engineered osteogenic-matrix after inclusion of TCP or Laponite at day 21. Significant upregulation of OCN and OPN was observed in the osteogenic niche after combination of the angiogenic niche and osteogenic niche (Combo) (**Figure 6e**). This is consistent with previous literature showing that co-cultures of hMSC and endothelial cells result in an increased osteogenic differentiation due to growth factor interactions.<sup>[10, 20, 21]</sup> The results indicated that while the HUVECs/hMSCs-laden micropatterned GelMA held a great potential to generate highly organized vascular networks with a level of maturity indicated by the presence of VE-Cadherin between neighboring endothelial cells (**Figure 6b**), the POB-encapsulated GelMA could maintain their regular differentiation functions (**Figure 6e**) and generate osteogenesis simultaneously in culture medium, which does not contain osteogenic factors.



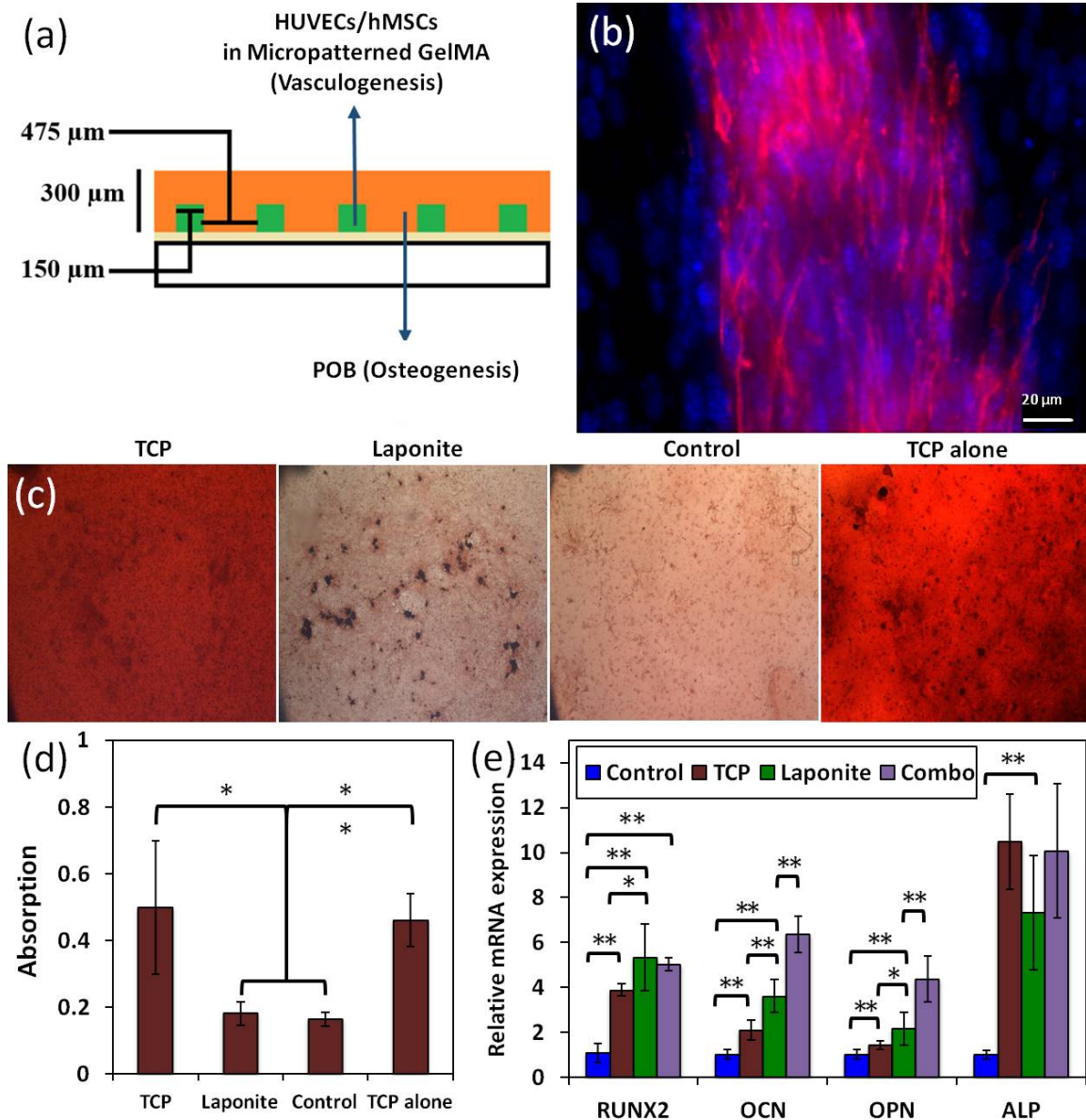


**Fig 6: Osteogenic characterization of microconstruct.** (a) Schematic of vasculo-ostegenic construct. (b) Expression of endothelial intercellular junctional protein VE-cadherin after 2 weeks culture. (c) Representative Alizarin Red images of POB-laden osteogenic GelMA constructs with TCP or Laponite. (d) Significantly higher calcium deposition was observed in the samples with TCP. \* $P < 0.05$ , as compared, however this difference was due to the presence of calcium in TCP as confirmed by TCP sample without cells. (e) qPCR analysis indicated that osteogenic genes OCN, RUNX2, OPN and ALP were expressed in the engineered osteogenic-matrix and significant upregulation of OCN and OPN was observed in the osteogenic niche after combination of angiogenic niche and osteogenic niche (Combo) at day 21.

#### 4. Conclusions

This study presents a method to pattern vascular structures within a tissue engineered bone construct using a two-step photopolymerization approach. This approach offers a high level of control over the organization of the vascular structures, especially when patterns with a width of 150  $\mu\text{m}$  or less are used. By adapting the design of the photomasks used, this potentially enables the design of complex vascular patterns resembling for instance a vascular tree. hMSCs present in the angiogenic niche differentiate towards mural cells and stabilize the vascular structures. By adding Laponite silicate nanoparticles to the osteogenic niche, cells in the osteogenic niche maintain their osteogenic potential, even when cultured in media not supplemented with osteogenic factors. The osteogenic differentiation is further increased by the presence of angiogenic niche containing endothelial cells.

This study shows the potential of engineering a tissue containing two separate niches, which are optimized for their respective function. By localizing tissue developmental cues, this enables the formation of multiple tissue structures within a single construct cultured in a single medium. This is an important advancement for multi-structural tissue engineering where the inclusion of a vascular or neural network becomes ever more important.

#### 5. Experimental Section

*Synthesis of GelMA and Prepolymer:* GelMA was synthesized according to our previous work<sup>[31, 46]</sup>. Medium methacrylation degree of GelMA ( $53.8 \pm 0.5\%$ ) was selected due to its robust mechanical properties and low mass swelling ratio at low UV exposure which provides high cell viability<sup>[31, 54]</sup>. Briefly, GelMA was produced by dissolving 10% (w/v) type A gelatin derived from porcine skin (Sigma-Aldrich) into Dulbecco's phosphate buffered saline (DPBS) (GIBCO) by stirring at 50 °C. Then 5 mL methacrylic anhydride (MA) (Sigma-Aldrich) was added dropwise to the suspension at a rate of 0.5 mL  $\text{min}^{-1}$  and allowed to stir for 3 h at 50 °C. The addition of methacrylate groups to the amine- side groups

of gelatin created a photopolymerizable hydrogel <sup>[31, 40]</sup>. Subsequently, the reaction was stopped by diluting the solution five-fold with DBPS at 50 °C. The GelMA solution was then dialyzed against distilled water for 10 days using a 12-14 kDa cutoff dialysis tube (Spectrum Laboratories) to remove salts and unreacted MA. After freezing the GelMA solution at -80 °C a white GelMA foam was obtained by lyophilization and stored at -20°C. GelMA prepolymer solution was prepared by mixing freeze-dried GelMA foam at concentrations of 5% and 8% (w/v) and the photoinitiator [2-hydroxy-1-(4-(hydroxyethoxy) phenyl)-2- methyl-1-propanone, Irgacure 2959] (CIBA Chemicals) in DPBS at 80 °C.

*Micro patterning Process:* A two-step microfabrication protocol was developed with angiogenic and osteogenic niches in a single construct. First, to make GelMA prepolymer adhere to the glass slides (1 cm<sup>2</sup>), free methacrylate groups were created on the slides by treating the glass with 3-(trimethoxysilyl)propyl methacrylate (TMSPMA) (Sigma) according to a previously described protocol. <sup>[31]</sup> TMSPMA-treated slides were sterilized by UV light prior to experiments. To generate the micropatterned angiogenic niche, 20 µL GelMA 5% (w/v) solution containing GFP-HUVECs and hMSCs at a cell densities of  $2.5 \times 10^6$  and  $2.5 \times 10^6$  cells/mL, respectively, was added between the 150 µm spacers on a petri dish and covered with a TMSPMA-treated glass slide. To create organized an array of GelMA micropatterns on the glass a photomask with 475 µm spacing and 50, 150 and 300 µm beam size (designed by AutoCAD software) was positioned on top of the slide and the cell-encapsulated GelMA was photocrosslinked with UV light positioned beneath the device (OmniCure® Series 2000) with 100 mW/cm<sup>2</sup> for 35 s. A photomask is a two dimensional (2D) pattern printed onto a transparent sheet, designed such that light only passes through the mask in specific patterns (**Figure 1**). <sup>[37]</sup> The osteogenic niche was overlaid on the micropatterned GelMA on TMSPMA glass as a layer of POB laden GelMA 8% (w/v) at a cell density of  $5 \times 10^6$  cells/mL with 300 µm spacers and polymerized with UV light with 100 mW/cm<sup>2</sup> for 35 s. The GelMA/POB layer filled the spaces between the micropatterned angiogenic lines intended for bone formation and generated a construct for osteogenesis through

differentiation of POB to mature osteoblasts in the presence of optimized endothelial cell growth media (**Figure 1**). The construct was then cultured in the EGM media.

*Cell Culture:* Green fluorescent protein (GFP)-expressing human umbilical vein endothelial cells (HUVECs) (Lonza), was cultured in basal medium (EBM-2; Lonza) supplemented with endothelial growth BulletKit (EGM-2; Lonza). Human bone marrow-derived mesenchymal stem cells (hMSCs) (Lonza) was cultured in Minimum Essential Medium Alpha (MEM Alpha, Life Technologies), supplemented with 2 mM L-glutamine (Life Technologies), 0.2 M ascorbic acid (Life Technologies), 1 ng/mL basic fibroblast growth factor (bFGF, Life Technologies), 10% fetal bovine serum (FBS, Life Technologies) and 1% Antibiotic-Antimycotic (Gibco). MC3T3 preosteoblast cells were cultured using the growth media, containing Minimum Essential Medium Alpha supplemented with 10% fetal bovine serum and 1% Antibiotic-Antimycotic. The cells with passage numbers between 3 and 6 were used in the experiments. The media was changed every two days and the cells were passaged at 80% confluency. For cell encapsulation, the cells were trypsinized, counted and homogenously mixed with 37 °C GelMA solution and used immediately.

*Quantification of cellular alignment:* The cell-laden hydrogels were fixed in 4% paraformaldehyde solutions in DPBS and stained with phalloidin (Alexa-Fluor 488, Invitrogen) and DAPI (Invitrogen) according to the manufacturer's instructions. Briefly, the specimen were permeabilized with 0.3% (v/v) Triton X-100 for 15 min, blocked by using 5% (w/v) bovine serum albumin (BSA) for 60 min before staining. Alignment analysis was performed using fluorescent images with an inverted fluorescence microscope (Nikon TE 2000-U, Nikon instruments, USA) to reveal filamentous actin and cell nuclei. The cellular alignment within patterned regions of the hydrogels was quantified based on cytoskeletal actin filaments-stained fluorescent images according to a previously described procedure<sup>[35, 47, 55]</sup>. To quantify the overall cellular alignment for each sample, the alignment

of actin filaments in the encapsulated was grouped in  $10^\circ$  increments and the alignment distributions were normalized to the respective preferred orientation to defined mean orientation. The measurements were performed using the built-in functions of ImageJ software (NIH) (6 images for each sample) (**Figure 2**). Confocal microscopy was used to evaluate actin cytoskeletal organization of the micropatterns (**video clip S1**).

*Cell Viability and Proliferation Assay:* *In vitro* qualitative analysis of viability of the encapsulated cells in GelMA constructs was performed using the fluorescence-based LIVE/DEAD<sup>®</sup> viability/cytotoxicity assay kit (Invitrogen) consisting intracellular green-fluorescent calcein AM and red-fluorescent ethidium homodimer. Initially a solution containing two components at 0.5  $\mu\text{L}/\text{mL}$  of calcein and 2  $\mu\text{L}/\text{mL}$  ethidium homodimer were dissolved in DPBS, respectively. At each time point the media were removed and the hydrogels covered with cells were rinsed with DPBS and subsequently 1 mL of the solution was added to each sample. After incubation for 30 min at ambient condition, the samples were imaged with 10X magnifications using an inverted fluorescent microscope (Nikon TE 2000-U, Nikon instruments, USA). Total number of cells (red and green) and number of live cells (green) were counted using ImageJ software (NIH). Finally, cell viability was quantified by dividing the number of live cells by total number of cells. The calculations were based on three independent samples and reported based on the mean  $\pm$  standard deviation (**Figure 3**). Cell proliferation was assessed using resazurin-based PrestoBlue<sup>®</sup> assay (Invitrogen), a non-toxic metabolic indicator for viable cells. Briefly, after each time point the culture medium was removed and the samples were rinsed with DPBS. Subsequently the medium containing 10% PrestoBlue<sup>®</sup> reagent was added to each well and incubated at 37  $^\circ\text{C}$  for 1 h. The samples with reagent but no cells served as the blank control. The fluorescence of the reduced PrestoBlue<sup>®</sup> dye was read at 570 (excitation) and 600 nm (emission) with a microplate reader (Biotek, USA), and all values were corrected based on blank control. Three replicates were analyzed for 1, 3 and 5 days and growth was plotted based on the mean  $\pm$  standard deviation (6 images for each

sample).

*Immunostaining:* The angiogenic activity of HUVECs/hMSCs co-culture was investigated using fluorescent microscopy to assess anti-CD31 and  $\alpha$ -SMA expression. The samples were rinsed in DPBS and fixed in 4% paraformaldehyde solution in DPBS for 20 min. Subsequently the cell membranes were permeabilized in 0.1% Triton X-100 in DPBS for 15 min and washed with DPBS for 3 times. The samples were then blocked with 1% (w/v) BSA in DPBS for 1 h, followed by primary antibody staining with 1/40 dilution of rabbit monoclonal anti-CD31 antibody (Abcam) and 1/100 dilution of mouse monoclonal anti-alpha smooth muscle actin antibody (Abcam) in 0.1% BSA blocking solution overnight at 4 °C. The samples were washed in DPBS three times with 1 h intervals in between the washing steps. After primary antibody staining, the samples were incubated in 1/200 dilution of Alexa Fluor-488 conjugated goat anti-rabbit (Abcam) and 1/200 dilution of Alexa Fluor-594 conjugated goat anti-mouse secondary antibodies (Abcam) in 0.1% BSA in DPBS for 2 h at ambient condition . Subsequently, the samples were washed in DPBS three times with 1 h intervals in between the washing steps, followed by 1/1000 dilution DAPI staining for 5 min. After rinsing the samples with DPBS, fluorescent images were taken. The relative surface area of coverage for stains was quantified with the ImageJ software (NIH). The images for the expression of VE-cadherein (Abcam) as the primary antibody within the micropatterned regions of GelMA hydrogel constructs were assessed after 21 days culture using the same protocol as described above.

*Mineralization:* The cell-laden constructs were fixed using 4% paraformaldehyde for 30 min at room temperature after washing twice with PBS. Subsequently, the samples were stained for 10 min with 2% Alizarin Red (Sigma- Aldrich) solution of which the pH was adjusted to 4.1-4.3 using ammonium hydroxide. The samples were then washed with distilled water several times to remove all untreated reagents. Stained slides were visualized by phase microscopy using an inverted microscope (Nikon). To

quantify mineralization, the sample were dissolved in 200  $\mu$ L ammonia solution (10%) and kept overnight. Following vortexing, the solution was heated at 80 °C for 10 min and centrifuged at 20000  $\times$ g for 15 min. Afterward 75  $\mu$ L of 10% ammonia solution was added to each solution and the absorbance was read at 405 nm.

*RNA isolation and quantitative real-time PCR (qPCR):* Total RNA was extracted from samples using TRIzol (Invitrogen) and 1  $\mu$ g of total RNA was used for cDNA synthesis with SuperScript™ III First-Strand Synthesis SuperMix (Invitrogen). For quantitative real-time PCR analysis, gene-specific primers were designed to amplify mouse RUNX2, OPN, OCN, ALP, and the housekeeping gene glyceraldehyde 3-phosphate dehydrogenase (GAPDH). Primer pairs are as follows: RUNX2 (5'-AGG TTG GAG GCA CAC ATA GG-3', 5'-TTG ACC TTT GTC CCA ATG C-3'), OPN (5'-AAG CAT CCT TGC TTG GGT TT-3', 5'-CAG GCT TAC CTT GGC TGG TTT-3'), OCN (5'-ATT TAG GAC CTG TGC TGC CC-3', 5'-GCA GAG AGA GAG GAC AGG GA-3'), ALP (5'-CAG GCC GCC TTC ATA AGC A-3', 5'-AAT TGA CGT TCC GAT CCT GC-3'), and GAPDH (5'-ACA CAT TGG GGG TAG GAA CA-3', 5'-AAC TTT GGC ATT GTG GAA GG-3'). All amplifications were performed in a final reaction mixture (20  $\mu$ L) containing 1 final concentration of Bio-Rad SYBR Green Master Mix (Bio-Rad, Hercules, CA), 500 nmol/L of gene-specific primers, and 1  $\mu$ L of template, using the following conditions: an initial denaturation at 95 °C for 1 min, followed by 45 cycles of 95 °C for 15 sec, 56 °C for 15 sec, and 72 °C for 15 sec, with a final extension at 72 °C for 5 min. After amplification, the baseline and threshold levels for each reaction were determined using CFX Manager Software (Bio-Rad). For validation of polymerase chain reaction (PCR), amplified products were separated on 1% agarose gels and visualized by ethidium bromide staining. The relative quantification in gene expression was determined using the  $2^{-\Delta\Delta C_t}$  method. [56]

*Statistical Analysis:* The statistical significance was determined by an independent Student t-test

for two groups of data or analysis of variance (ANOVA). Data were calculated as mean  $\pm$  standard deviation (SD) for six replicates and  $p$  values were presented as statistically significant and highly significant as \*  $p < 0.05$ , \*\*  $p < 0.01$  respectively.

## 6. Acknowledgements

The authors acknowledge funding from the National Science Foundation (EFRI-1240443), IMMODGEL (602694), and the National Institutes of Health (EB012597, AR057837, DE021468, HL099073, AI105024, AR063745). JR was supported by the People Programme (Marie Curie Actions) of the European Union's Seventh Framework Programme (FP7/2007–2013) under REA grant agreement n°622294.

## References

- [1] Á. Mercado-Pagán, A. Stahl, Y. Shanjani, Y. Yang, *Ann Biomed Eng* 2015, 43, 718.
- [2] M. I. Santos, R. L. Reis, *Macromolecular Bioscience* 2010, 10, 12.
- [3] C. F. Lord, M. C. Gebhardt, W. W. Tomford, H. J. Mankin, *The Journal of Bone & Joint Surgery* 1988, 70, 369.
- [4] N. A. Beckmann, S. Mueller, M. Gondan, S. Jaeger, T. Reiner, R. G. Bitsch, *The Journal of Arthroplasty* 2015, 30, 249.
- [5] H. Nie, M.-L. Ho, C.-K. Wang, C.-H. Wang, Y.-C. Fu, *Biomaterials* 2009, 30, 892.
- [6] K. J. L. Burg, S. Porter, J. F. Kellam, *Biomaterials* 2000, 21, 2347.
- [7] O. Tsigkou, I. Pomerantseva, J. A. Spencer, P. A. Redondo, A. R. Hart, E. O'Doherty, Y. Lin, C. C. Friedrich, L. Daheron, C. P. Lin, C. A. Sundback, J. P. Vacanti, C. Neville, *Proceedings of the National Academy of Sciences of the United States of America* 2010, 107, 3311.
- [8] S. Bose, M. Roy, A. Bandyopadhyay, *Trends in Biotechnology* 2012, 30, 546.
- [9] M. K. Narbat, M. S. Hashtjin, M. Pazouki, *Iranian Journal of Biotechnology (IJB)* 2006, 4.
- [10] J. Ma, S. K. Both, F. Yang, F. Z. Cui, J. Pan, G. J. Meijer, J. A. Jansen, J. J. van den Beucken, *Stem cells translational medicine* 2014, 3, 98.
- [11] S. P. Bruder, B. S. Fox, *Clinical Orthopaedics and Related Research* 1999, 367, S68.
- [12] L. H. Nguyen, N. Annabi, M. Nikkhah, H. Bae, L. Binan, S. Park, Y. Kang, Y. Yang, A. Khademhosseini, *Tissue Engineering Part B: Reviews* 2012, 18, 363.
- [13] Y. Liu, B. Moller, J. Wiltfang, P. H. Warnke, H. Terheyden, *Tissue engineering. Part A* 2014, 20, 3189.
- [14] R. K. Jain, P. Au, J. Tam, D. G. Duda, D. Fukumura, *Nat Biotech* 2005, 23, 821.



- [15] L. Krishnan, N. Willett, R. Guldborg, *Ann Biomed Eng* 2014, 42, 432.
- [16] E. C. Novosel, C. Kleinhaus, P. J. Kluger, *Advanced Drug Delivery Reviews* 2011, 63, 300; M. O. Wang, C. E. Vorwald, M. L. Dreher, E. J. Mott, M.-H. Cheng, A. Cinar, H. Mehdizadeh, S. Somo, D. Dean, E. M. Brey, J. P. Fisher, *Advanced Materials* 2015, 27, 138.
- [17] L. H. Nguyen, N. Annabi, M. Nikkhah, H. Bae, L. Binan, S. Park, Y. Kang, Y. Yang, A. Khademhosseini, *Tissue engineering. Part B, Reviews* 2012, 18, 363.
- [18] J. García, A. García, *Drug Deliv. and Transl. Res.* 2015, 1.
- [19] N. Annabi, A. Tamayol, J. A. Uquillas, M. Akbari, L. E. Bertassoni, C. Cha, G. Camci-Unal, M. R. Dokmeci, N. A. Peppas, A. Khademhosseini, *Advanced Materials* 2014, 26, 85.
- [20] C. Correia, W. L. Grayson, M. Park, D. Hutton, B. Zhou, X. E. Guo, L. Niklason, R. A. Sousa, R. L. Reis, G. Vunjak-Novakovic, *PloS one* 2011, 6, e28352.
- [21] J. M. Kanczler, R. O. Oreffo, *European cells & materials* 2008, 15, 100.
- [22] S. Patan, in *Angiogenesis in Brain Tumors*, Vol. 117 (Eds: M. Kirsch, P. Black), Springer US, 2004, 3.
- [23] B. V. Slaughter, S. S. Khurshid, O. Z. Fisher, A. Khademhosseini, N. A. Peppas, *Advanced materials (Deerfield Beach, Fla.)* 2009, 21, 3307.
- [24] C. S. Choong, D. W. Huttmacher, J. T. Triffitt, *Tissue engineering* 2006, 12, 2521.
- [25] R. Vattikuti, D. A. Towler, *American Journal of Physiology - Endocrinology and Metabolism* 2004, 286, E686.
- [26] D. M. Supp, K. Wilson-Landy, S. T. Boyce, *FASEB journal : official publication of the Federation of American Societies for Experimental Biology* 2002, 16, 797.
- [27] Y.-C. Chen, R.-Z. Lin, H. Qi, Y. Yang, H. Bae, J. M. Melero-Martin, A. Khademhosseini, *Advanced Functional Materials* 2012, 22, 2027.
- [28] Y. Kang, S. Kim, M. Fahrenholtz, A. Khademhosseini, Y. Yang, *Acta Biomaterialia* 2013, 9, 4906.
- [29] H. Kaji, "Biofabrication techniques for biologically relevant tissue models and drug delivery devices", presented at *Micro-NanoMechatronics and Human Science (MHS), 2012 International Symposium on*, 4-7 Nov. 2012, 2012.
- [30] Y. Zuo, W. Xiao, X. Chen, Y. Tang, H. Luo, H. Fan, *Chemical Communications* 2012, 48, 3170.
- [31] J. W. Nichol, S. T. Koshy, H. Bae, C. M. Hwang, S. Yamanlar, A. Khademhosseini, *Biomaterials* 2010, 31, 5536.
- [32] M. Kazemzadeh-Narbat, N. Annabi, A. Khademhosseini, ELSEVIER SCI LTD THE BOULEVARD, LANGFORD LANE, KIDLINGTON, OXFORD OX5 1GB, OXON, ENGLAND, 2015; P. Hassanzadeh, M. Kazemzadeh-Narbat, R. Rosenzweig, X. Zhang, A. Khademhosseini, N. Annabi, M. Rolandi, *Journal of Materials Chemistry B* 2016; A. Tamayol, A. H. Najafabadi, B. Aliakbarian, E. Arab-Tehrany, M. Akbari, N. Annabi, D. Juncker, A. Khademhosseini, *Advanced healthcare materials* 2015, 4, 2146.
- [33] M. Nikkhah, F. Edalat, S. Manoucheri, A. Khademhosseini, *Biomaterials* 2012, 33, 5230.
- [34] H. Qi, Y. Du, L. Wang, H. Kaji, H. Bae, A. Khademhosseini, *Advanced materials (Deerfield Beach, Fla.)* 2010, 22, 5276; J. Ramon-Azcon, S. Ahadian, R. Obregon, G. Camci-Unal, S. Ostrovidov, V. Hosseini, H. Kaji, K. Ino, H. Shiku, A. Khademhosseini, *T. Matsue, Lab on a Chip* 2012, 12, 2959;

- N. Annabi, K. Tsang, S. M. Mithieux, M. Nikkhah, A. Ameri, A. Khademhosseini, A. S. Weiss, *Advanced Functional Materials* 2013, 23, 4950; W. Xiao, J. He, J. W. Nichol, L. Wang, C. B. Hutson, B. Wang, Y. Du, H. Fan, A. Khademhosseini, *Acta Biomaterialia* 2011, 7, 2384; R. Gauvin, Y. C. Chen, J. W. Lee, P. Soman, P. Zorlutuna, J. W. Nichol, H. Bae, S. Chen, A. Khademhosseini, *Biomaterials* 2012, 33, 3824.
- [35] J. Ramon-Azcon, S. Ahadian, R. Obregon, G. Camci-Unal, S. Ostrovidov, V. Hosseini, H. Kaji, K. Ino, H. Shiku, A. Khademhosseini, T. Matsue, *Lab Chip* 2012, 12, 2959.
- [36] H. Aubin, J. W. Nichol, C. B. Hutson, H. Bae, A. L. Sieminski, D. M. Crokek, P. Akhyari, A. Khademhosseini, *Biomaterials* 2010, 31, 6941.
- [37] T. I. Son, M. Sakuragi, S. Takahashi, S. Obuse, J. Kang, M. Fujishiro, H. Matsushita, J. Gong, S. Shimizu, Y. Tajima, Y. Yoshida, K. Suzuki, T. Yamamoto, M. Nakamura, Y. Ito, *Acta Biomaterialia* 2010, 6, 4005.
- [38] N. Koike, D. Fukumura, O. Gralla, P. Au, J. S. Schechner, R. K. Jain, *Nature* 2004, 428, 138; J. M. Melero-Martin, M. E. De Obaldia, S. Y. Kang, Z. A. Khan, L. Yuan, P. Oettgen, J. Bischoff, *Circulation research* 2008, 103, 194.
- [39] Y.-Q. Yang, Y.-Y. Tan, R. Wong, A. Wenden, L.-K. Zhang, A. B. M. Rabie, *In J Oral Sci* 2012, 4, 64.
- [40] H. Bae, A. S. Puranik, R. Gauvin, F. Edalat, B. Carrillo-Conde, N. A. Peppas, A. Khademhosseini, *Science Translational Medicine* 2012, 4, 160ps23.
- [41] M. M. Deckers, M. Karperien, C. van der Bent, T. Yamashita, S. E. Papapoulos, C. W. Lowik, *Endocrinology* 2000, 141, 1667.
- [42] H. Yuan, Z. Yang, Y. Li, X. Zhang, J. D. De Bruijn, K. De Groot, *Journal of Materials Science: Materials in Medicine* 1998, 9, 723; C. Weinand, I. Pomerantseva, C. M. Neville, R. Gupta, E. Weinberg, I. Madisch, F. Shapiro, H. Abukawa, M. J. Troulis, J. P. Vacanti, *Bone* 2006, 38, 555.
- [43] A. K. Gaharwar, S. M. Mihaila, A. Swami, A. Patel, S. Sant, R. L. Reis, A. P. Marques, M. E. Gomes, A. Khademhosseini, *Adv Mater* 2013, 25, 3329; J. I. Dawson, J. M. Kanczler, X. B. Yang, G. S. Attard, R. O. Oreffo, *Advanced materials (Deerfield Beach, Fla.)* 2011, 23, 3304.
- [44] R. Gauvin, Y.-C. Chen, J. W. Lee, P. Soman, P. Zorlutuna, J. W. Nichol, H. Bae, S. Chen, A. Khademhosseini, *Biomaterials* 2012, 33, 3824; H. Shin, B. D. Olsen, A. Khademhosseini, *Biomaterials* 2012, 33, 3143.
- [45] S. R. Shin, B. Aghaei-Ghareh-Bolagh, T. T. Dang, S. N. Topkaya, X. Gao, S. Y. Yang, S. M. Jung, J. H. Oh, M. R. Dokmeci, X. S. Tang, A. Khademhosseini, *Advanced materials (Deerfield Beach, Fla.)* 2013, 25, 6385.
- [46] E. B. Luiz, C. C. Juliana, M. Vijayan, L. C. Ana, S. B. Nupura, A. A. Wesleyan, Z. Pinar, E. V. Nihal, M. G. Amir, R. D. Mehmet, K. Ali, *Biofabrication* 2014, 6, 024105.
- [47] M. Nikkhah, N. Eshak, P. Zorlutuna, N. Annabi, M. Castello, K. Kim, A. Dolatshahi-Pirouz, F. Edalat, H. Bae, Y. Yang, A. Khademhosseini, *Biomaterials* 2012, 33, 9009.
- [48] G. E. Davis, C. W. Camarillo, *Experimental cell research* 1996, 224, 39.
- [49] R. B. Vernon, E. H. Sage, *The American journal of pathology* 1995, 147, 873; D. Manoussaki, S. R. Lubkin, R. B. Vernon, J. D. Murray, *Acta biotheoretica* 1996, 44, 271.

- [50] C. M. Nelson, R. P. Jean, J. L. Tan, W. F. Liu, N. J. Sniadecki, A. A. Spector, C. S. Chen, *Proceedings of the National Academy of Sciences of the United States of America* 2005, 102, 11594; N. C. Rivron, E. J. Vrij, J. Rouwkema, S. Le Gac, A. van den Berg, R. K. Truckenmüller, C. A. van Blitterswijk, *Proceedings of the National Academy of Sciences* 2012, 109, 6886.
- [51] V. Hosseini, P. Kollmannsberger, S. Ahadian, S. Ostrovidov, H. Kaji, V. Vogel, A. Khademhosseini, *Small* 2014, 10, 4851.
- [52] Y. C. Chen, R. Z. Lin, H. Qi, Y. Yang, H. Bae, J. M. Melero-Martin, A. Khademhosseini, *Adv Funct Mater* 2012, 22, 2027.
- [53] N. Huebsch, P. R. Arany, A. S. Mao, D. Shvartsman, O. A. Ali, S. A. Bencherif, J. Rivera-Feliciano, D. J. Mooney, *Nat Mater* 2010, 9, 518.
- [54] C. Cha, S. R. Shin, X. Gao, N. Annabi, M. R. Dokmeci, X. S. Tang, A. Khademhosseini, *Small* 2014, 10, 514.
- [55] A. Suci, G. Civelekoglu, Y. Tardy, J. J. Meister, *Bulletin of mathematical biology* 1997, 59, 1029; S. Ostrovidov, S. Ahadian, J. Ramon-Azcon, V. Hosseini, T. Fujie, S. P. Parthiban, H. Shiku, T. Matsue, H. Kaji, M. Ramalingam, H. Bae, A. Khademhosseini, *Journal of Tissue Engineering and Regenerative Medicine* 2014, n/a.
- [56] K. J. Livak, T. D. Schmittgen, *Methods* 2001, 25, 402.

## **Supporting Information**

### **Engineering multicomponent hydrogel constructs for creating 3D vascularized bones**

*Mehdi Kazemzadeh-Narbat, Jeroen Rouwkema, Nasim Annabi, Hao Cheng, Masoumeh Ghaderi, Byung-Hyun Cha, Mansi Aparnathi, Akbar Khalilpour, Batzaya Byambaa, Esmail Jabbari, Ali Tamayol\*, Ali Khademhosseini\**

**Video S1:** A video clip showing the formation of cord-like structure of actin filaments stained HUVECs/MCSs-laden micropatterned GelMA constructs. Optimum 3D cord-like structure was observed at 150  $\mu\text{m}$ .